# A Photometric Study of ASAS J184708-3340.2: an Eclipsing Binary with Total Eclipses

**Robert C. Berrington**
*Ball State University, Dept. of Physics and Astronomy, Muncie, IN 47306; rberring@bsu.edu*

**Erin M. Tuhey**
*Ball State University, Dept. of Physics and Astronomy, Muncie, IN 47306; emtuhey@bsu.edu*

*Received July 22, 2014; revised August 20, 2014 and May 16, 2015; accepted May 26, 2015*

**Abstract** We present new multi-band differential aperture photometry of the eclipsing variable star ASAS J184708-3340.2. The light curves are analyzed with the Wilson-Devinney model to determine best-fit stellar models. Our models show that ASAS J184708-3340.2 is consistent with an overcontact eclipsing binary (W Ursae Majoris) system with total eclipses.

## 1. Introduction

The All Sky Automated Survey (Pojmański 1997; ASAS) catalog entry star 184708-3340.2 (R.A. $18^h$ $47^m$ $8^s$, Dec. –33º 40' 12" (J2000.0)) was originally classified as an eclipsing contact binary system (EC) with a period of P = 0.28174 day by Pojmański and Maciejewski (2005). The ASAS is a large-area photometric sky survey covering the entire southern hemisphere and a portion of the northern hemisphere ($\delta < 28º$) (Pojmański 1997). The survey provides continuous photometric and simultaneous monitoring of bright sources ($V \lesssim 14$ and $I \lesssim 13$) in both the V and I bands (Pojmański 2002). Currently, only the Johnson V band data have been made available to the public (http://www.astrouw.edu.pl/asas/). A convenient web-based interface accessing the classification database (Pojmański 2002, 2003; Pojmański and Maciejewski 2004, 2005; Pojmański *et al.* 2005) of all large-amplitude variable stars southward of declination –28º is provided, and reports a 13.27 V-band magnitude and V-band variability amplitude of 0.68 magnitude for ASAS J184708-3340.2. Because of the large area coverage of the survey, temporal resolution of the V and I band photometry is not fine enough to calculate times of minima for these short-period systems, and makes a detailed photometric study of short-period variable systems difficult.

In this paper we present a new extensive photometric study of ASAS J184708-3340.2. The paper is organized as follows. Observational data acquisition and reduction methods are presented in section 2. Time analysis of the photometric light curve and Wilson-Devinney (WD) models is presented in section 3. Discussion of the results and conclusions is presented in section 4.

## 2. Observational data

We present new three-filter differential aperture photometry of the eclipsing variable star ASAS J184708-3340.2. The data were taken by the SARA-South 0.6-meter telescope located at the Cerro Tololo Inter-American Observatory (CTIO). All exposures were acquired by the Astronomical Research Cameras (ARC), Inc. camera, which uses the thinned, back-illuminated E2V CCD42-40 CCD that contains a 2k × 2k array of 13.5μm pixels, and were taken through the Johnson-Cousins B, V, and R ($R_C$) filters on the nights of June 22, 2013 (JD 2456465), and July 4, 2013 (JD 2456477), with 2 × 2 on-chip binning to expedite chip readout times. All images were bias and dark current subtracted, and flat field corrected using the CCDRED reduction package found in the Image Reduction and Analysis Facility (IRAF; distributed by the National Optical Astronomy Observatories (http://iraf.net/), version 2.16. All photometry presented is differential aperture photometry and was performed on the target eclipsing candidate and two comparison standards by the AIP4WIN (v2.2.0) photometry package (Berry and Burnell 2005). Over the two nights a total of 154 were images were taken in B, 155 images in V, and 157 images in R. Figure 1 shows a digitized sky survey POSS2/UKSTU red image (https://archive.stsci.edu/cgi-bin/dss_form) with the eclipsing star candidate and

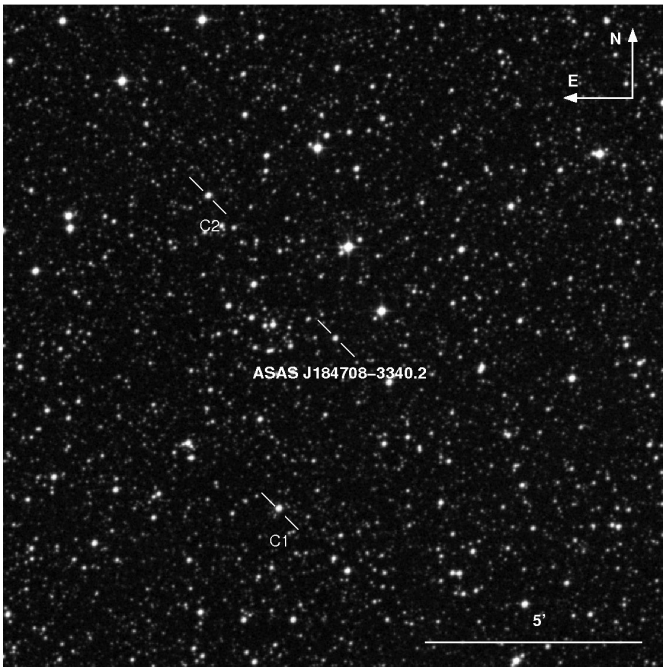


Figure 1. Star field containing the variable star ASAS J184708-3340.2. The location of the variable star is shown along with the comparison (C1) star and the check (C2) star used to calculate the differential magnitudes reported in Figure 2.

the two comparison stars marked, with the primary comparison star labeled C1 and the secondary comparison (check) star labeled C2. The folded light curves (see section 3.1) for the instrumental differential B, V, and $R_C$ magnitudes are shown in Figure 2, and are defined as the variable star magnitude minus C1 (Variable – C1). Also shown (bottom panel) in Figure 2 is the differential V magnitude of C1 minus C2. The comparison light curve was inspected for variability. None was found.

Because of the magnitude range of ASAS J184708-3340.2, the required exposure lengths necessary to obtain the targeted signal-to-noise ratio for the variable meant the stars with accurately measured Johnson-Cousins B, V, and $R_c$ magnitudes were saturated. To solve this issue, we took several exposures with shortened exposure times that did not saturate the brighter stars with accurately known magnitudes. These exposures allowed us to calibrate the magnitudes for C1 and C2. The stars used for this calibration were the Tycho stars TYC 7412-1069-1, TYC 7412-1794-1, and TYC 7412-1940-1 (Høg *et al.* 2000).

Measured instrumental B and V differential magnitudes for C1 and the aforementioned Tycho stars were converted to Johnson B and V magnitudes by comparison with known calibrated magnitudes of the Tycho stars. The calibrated magnitudes were averaged together after individual values were found to be consistent with each other ($< 1.5\sigma$) in both the Johnson B and V bands. The star C1 was found to have measured Johnson B and V magnitude, of $13.90 \pm 0.10$ and $12.77 \pm 0.12$, respectively. The calibrated V light curve with the (B–V) color index versus orbital phase is shown in Figure 3. Error bars have been removed for clarity. The orbital phase ($\Phi$) is defined as:

$$\Phi = \frac{T - T_0}{P} - \text{Int}\left(\frac{T - T_0}{P}\right), \qquad (1)$$

where $T_0$ is the ephemeris epoch and is the time of minimum of a primary eclipse. Throughout this paper we will use the value of 2456465.595055 for $T_0$. The variable $T$ is the time of observation, and the period of the orbit is given by $P$. The value of $\Phi$ typically ranges from a minimum of 0 to a maximum of 1.0. We can also define negative orbital phase values by the relation $\Phi - 1$. All light curve figures will plot phase values (–0.6,0.6). Simultaneous B and V magnitudes are used to determine ($B–V$) colors by linear interpolationbetween measured B magnitudes.

## 3. Analysis

### 3.1. Period analysis and ephemerides

Heliocentric Julian dates (HJD) for the observed times of minimum were calculated for each of the B-, V-, and $R_c$-band light curves shown in Figure 2 for all observed primary and secondary minima. A total of one primary eclipse and two secondary eclipses were observed for each band. The times of minimum were determined by the algorithm described by Kwee and van Woerden (1956). Times of minimum from differing band passes were compared and no significant offsets or wavelength dependent trends were observed. Times of minimum from each of the band passes were averaged together and reported in Table 1 along with 1σ error bars.

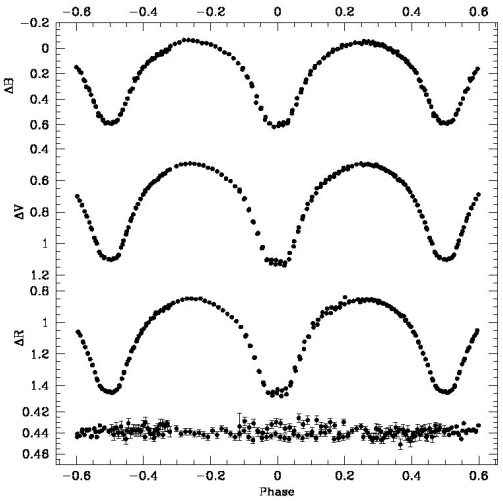


Figure 2. Folded light curves for differential aperture Johnson-Cousins B-, V-, and $R_C$-band magnitudes. Phase values are defined by Equation 1. Top three panels show the folded light curves for Johnson B (top panel), Johnson V (middle panel), and Cousins $R_C$ (bottom panel) magnitudes. Bottom panel shows differential Johnson V-band magnitudes for the comparison minus the check star. All error bars are 1σ error bars, and for the top three panels are smaller than the point size. Repeated points do not show error bars (points outside the phase range of (–0.5,0.5)).

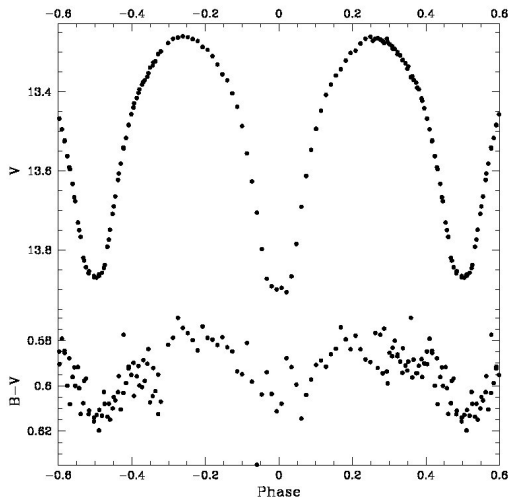


Figure 3. Folded light curve for differential aperture Johnson V band magnitudes (top panel) and (B–V) color (bottom panel) versus orbital phase. Phase values are defined by Equation 1. Error bars are not shown for clarity. All ($B–V$) colors are calculated by subtracting linearly interpolated B magnitudes from measured V magnitudes. Magnitudes calibration is discussed in section 2.

Light curves were inspected using the PERANSO (v2.51) software (CBA Belgium Observatory 2011) to determine the orbital period by applying the analysis of variance (ANOVA) statistic which uses periodic orthogonal polynomials to fit observed light curves (Schwarzenberg-Czerny 1996). Our best-fit orbital period was found to be $0.28179 \pm 0.00020$ day and is consistent ($< 1\sigma$) with the orbital period reported by Pojmański and Maciejewski (2005). The resulting linear ephemeris becomes:

$$T_{min} = 2456465.59506(22) + 0.28179(24)\ E. \quad (2)$$

where the variable $E$ represents the epoch number, and is a count of orbital periods from the epoch $T_0 = 2456465.59506$. Figure 2 shows the folded differential magnitudes versus orbital phase for ASAS J184708-3340.2 for the B, V, and $R_C$ Johnson-Cousins bands folded over the period determined by the current photometric study.

The observed minus calculated residual times of minimum ($O-C$) were determined from Equation 2 and are given in Table 1 along with 1σ error bars. The best-fit linear line determined by a linear regression to the ($O-C$) residual values is shown in Figure 4, and indicates a small correction to the period to a value of $0.2817412 \pm 0.0000008$ day. The newly determined period is consistent with our previously determined value from PERANSO at $< 1\sigma$ deviation. For all subsequent fitting the period of $0.2817412 \pm 0.0000008$ day will be assumed. The use of either period has no impact on the conclusions of this study.

3.2. Effective temperature and spectral type

Effective temperature and spectral type are estimated from the ($B-V$) color index values measured at orbital quadrature ($\Phi = \pm 0.25$) with a value of $(B-V) = 0.58 \pm 0.16$. The interstellar extinction estimate following Schlafly and Finkbeiner (2011) at the galactic coordinates for the object is $E(B-V) = 0.14$. The resulting intrinsic color becomes $(B-V)_0 = 0.44 \pm 0.16$. Effective temperatures and errors were estimated by Table 3 from Flower (1996) to be $T_{eff} = 6541 \pm 700$K. The corresponding stellar spectral type is F5 (Fitzgerald 1970).

3.3. Light curve analysis

All observations taken during this study were analyzed using the Physics of Eclipsing Binaries (PHOEBE) software package (v0.31a) (Prša and Zwitter 2005). The PHOEBE software package is a modeling package that provides a convenient, intuitive graphical user interface (GUI) to the WD code (Wilson and Devinney 1971).

All three Johnson-Cousins B, V, and $R_C$ bands were fit simultaneously by the following procedure. Initial fits were performed assuming a common convective envelope in direct thermal contact, resulting in a common surface temperature of $T_{eff} = 6541$K determined by the procedure discussed in section 3.1. Orbital period was set to the value of 0.2817412 day and not allowed to vary. Surface temperatures imply that the outer envelopes are convective, so the gravity brightening coefficients $B_1$ and $B_2$, defined by the flux dependency $F \propto g^{\beta}$, were initially set at the common value consistent with a convective envelope of 0.32 (Lucy 1967). The more recent studies of Alencar and Vaz (1997) and Alencar *et al.* (1999) predict values for $\beta \approx 0.4$. We initially set the standard stellar bolometric albedo $A_1 = A_2 = 0.5$ as suggested by Rucinski (1969) with two possible reflections.

The fitting procedure was used to determine the best-fit stellar models and orbital parameters from the observed light curves shown in Figure 2. Initial fits were performed assuming a common convective envelope in thermal contact, which assumes similar surface temperatures for both.

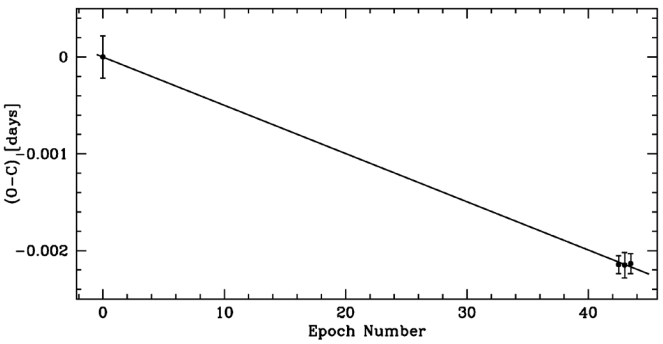


Figure 4. Observed minus calculated residual times of minimum ($O-C$) versus orbital epoch number. All point values are given in Table 1. Secondary times of minimum are plotted at half integer values, and all error bars are 1σ error bars. Solid curve shows the best-fit linear line determined by a linear regression fit to the ($O-C$) residual values.

Table 1. Calculated heliocentric Julian dates (HJD) for the observed times of minimum of ASAS J184708-3340.2.

| $T_{min}$ | *Eclipse* | *E* | *(O–C)* |
|---|---|---|---|
| 2456465.59506 ± 0.000218 | p | 0 | 0 ± 0.000218 |
| 2456477.56899 ± 0.000094 | s | 42.5 | –0.002145 ± 0.000094 |
| 2456477.70988 ± 0.000132 | p | 43 | –0.00215 ± 0.000132 |
| 2456477.85079 ± 0.000103 | s | 43.5 | –0.002135 ± 0.000103 |

*Notes: Calculated heliocentric Julian dates (HJD) for the observed times of minimum (column 1) with the type of minima (column 2). Observed minus Calculated (O-C) residual (column 4) values are given for the linear ephemeris given in Equation 2. All reported times are averaged from the individual B-, V-, and R-band times of minimum determined by the algorithm descried by Kwee and van Woerden (1956). All (O-C) values are given in units of days with primary eclipse values determined from integral epoch numbers, and secondary eclipse values determined from half integral epoch numbers (column 3).*

After normalization of the stellar luminosity, the light curve was crudely fit by altering the stellar shape by fitting the Kopal (Ω) parameter. The Kopal parameter describes the equipotential surface that the stars fill. This defines the shape of the stars, and strongly influences the global morphology of the light curve.

After the fit could no longer be improved, we started to consider the other parameters to fit the light curve. These parameters included the effective temperature of the secondary star $T_{eff,2}$, the mass ratio $q = M_2 / M_1$, and the orbital inclination $i$ , and we varied them to improve the overall model fit. Minor improvement of the of the best-fit model could be achieved by decoupling stellar luminosities from $T_{eff}$. We interpreted this as the possibility that the stars could have differing surface temperatures. All further model fits were performed assuming the primary and secondary components might have differing surface temperatures, but did not include decoupling stellar luminosities from $T_{eff}$.

All model fits were performed with a limb darkening correction. PHOEBE allows for differing functional forms to be specified by the user. Late-type stars ($T_{eff} < 9000$K) are best described by the logarithmic law which was first suggested by Klinglesmith and Sobieski (1970), and later supported by the more recent studies of Diaz-Cordoves and Gimenez (1992) and van Hamme (1993). For all of our model fits, we assumed

a logarithmic limb darkening law. The values for the linear ($x_\lambda$) and non-linear ($y_\lambda$) coefficients were determined at each fitting iteration by the van Hamme (1993) interpolation tables.

Figures 5 through 7 show the folded Johnson B-, Johnson V-, and Cousins $R_C$-band light curves along with the synthetic light curve calculated by the best-fit model, respectively. The best-fit models were determined by the aforementioned fitting procedure. The parameters along with 1σ error bars describing this best-fit model are given in column 3 of Table 2.

The filling factor is defined by the inner and outer critical equipotential surfaces that pass through the $L_1$ and $L_2$ Lagrangian points of the system, and is given by the following equation:

$$\mathcal{F} = \frac{\Omega(L_1) - \Omega}{\Omega(L_1) - \Omega(L_2)} \quad (3)$$

where Ω is the equipotential surface describing the stellar surface, and $\Omega(L_1)$ and $\Omega(L_2)$ are the equipotential surfaces that pass through the Lagrangian points $L_1$ and $L_2$, respectively. For our system the these equipotential surfaces are $\Omega(L_1)$ = 5.958, and $\Omega(L_2)$ = 5.348. The best-fit model is consistent with an overcontact binary described by a filling factor $\mathcal{F}$ = 0.151, and consistent with an overcontact binary system. Graphical representations for the best-fit WD model is shown in Figure 8.

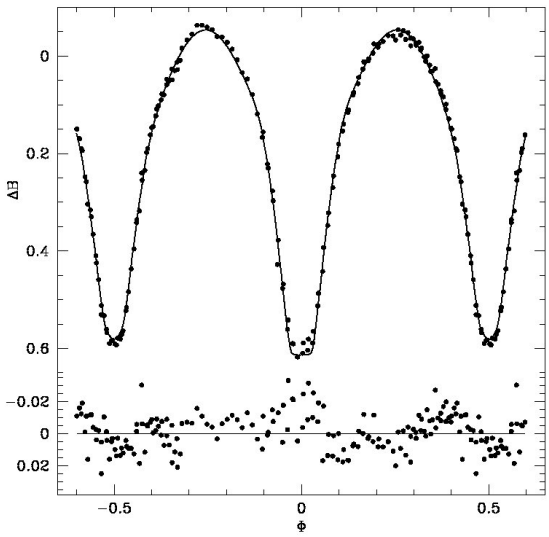


Figure 5. Best-fit WD model fit (solid curve) to the folded light curve for differential Johnson B-band magnitudes (top panel). The best-fit orbital parameters used to determine the light curve model are given in Table 2. The bottom panel shows residuals from the best-fit model (solid curve). Error bars are omitted from the points for clarity.

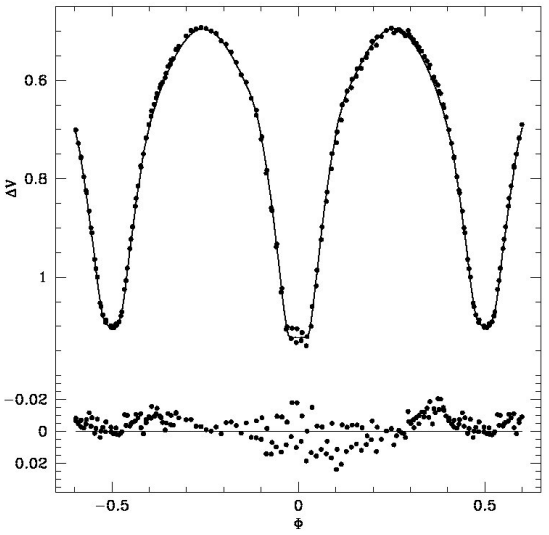


Figure 6. Best-fit WD model fit (solid curve) to the folded light curve for differential Johnson V-band magnitudes (top panel). The best-fit orbital parameters used to determine the light curve model are given in Table 2. The bottom panel shows residuals from the best-fit model (solid curve). Error bars are omitted from the points for clarity.

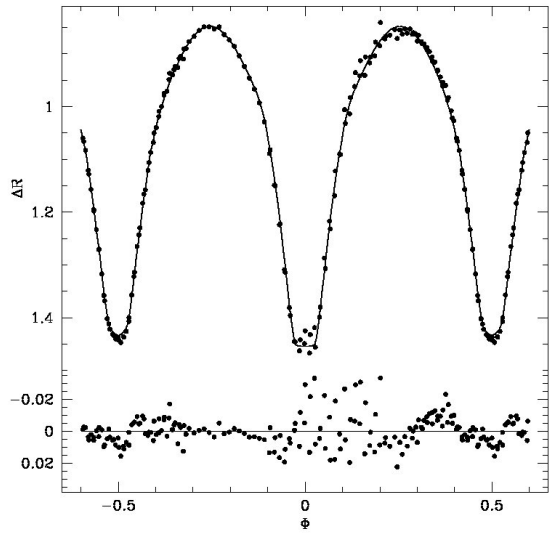


Figure 7. Best-fit WD model fit (solid curve) to the folded light curve for differential $R_C$-band magnitudes (top panel). The best-fit orbital parameters used to determine the light curve model are given in Table 2. The bottom panel shows residuals from the best-fit model (solid curve). Error bars are omitted from the points for clarity.

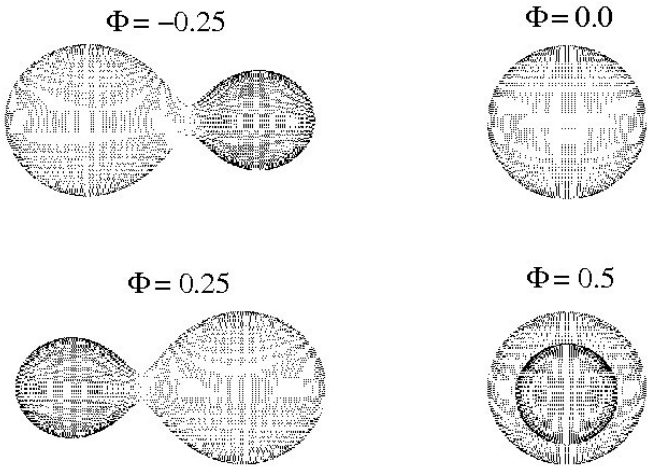


Figure 8. Graphical representation for the best-fit WD model. Orbital phase for each panel is given in the upper right corner. The best-fit orbital parameters used to determine the light curve model are given in Table 2.

Table 2. Model parameters for ASAS J184708-3340.2 determined by the best-fit WD model.

| *Parameter* | *Symbol* | *Value* |
|---|---|---|
| Period | P [days] | 0.2817412 ± 0.0000008 |
| Epoch | $T_0$ [HJD] | 2456465.59506 ± 0.0000008 |
| Inclination | i [º] | 88.1 ± 0.2 |
| Surface Temperature | $T_{eff,1}$ [K] | 6541 ± 700 |
| | $T_{eff,2}$ [K] | 6305 ± 700 |
| Surface Potential | Ω,2 [—] | 5.866 ± 0.003 |
| Mass Ratio | q [—] | 2.51 ± 0.01 |
| Luminosity | $[L_1/(L_1 + L_2)]B$ | 0.347 ± 0.001 |
| | $[L_1/(L_1 + L_2)]V$ | 0.338 ± 0.001 |
| | $[L_1/(L_1 + L_2)]R_C$ | 0.329 ± 0.001 |
| Limb Darkening | $x_{bol,1,2}$ | 0.64 |
| | $y_{bol,1,2}$ | 0.24 |
| | $x_{B,1,2}$ | 0.80 |
| | $y_{B,1,2}$ | 0.25 |
| | $x_{V,1,2}$ | 0.71 |
| | $y_{V,1,2}$ | 0.28 |
| | $x_{R,1,2}$ | 0.62 |
| | $y_{R,1,2}$ | 0.28 |

*Notes: Values for each parameter (column 1) along with brief descriptions (column 2) that specify the best-fit WD stellar model are given in column 3. Some parameters can be further specified by a the numerical value 1 for the primary stellar component, or 2 for the secondary stellar component. Fitting procedure is described in section 3.3. Surface potentials for both stars for contact/overcontact binaries is defined to be of equal value for both stars. Errors for surface temperatures ($T_{eff}$) were estimated from color values in Figure 3. All remaining errors are 1σ errors. Please note that the parameters $L_1$ and $L_2$ refer to the luminosities of primary and secondary components, respectively.*

## 4. Discussion and conclusions

Given the parameters in Table 2, we can estimate the distance to ASAS J184708-3340.2. Rucinski and Duerbeck (1997) determined that the absolute visual magnitude is given by

$$M_V = -4.44 \log_{10} (P) + 3.02 (B-V)_0 + 0.12 \quad (4)$$

to within an accuracy of ±0.22. The distance modulus of the system ($m - M$) = 9.38 for the value obtained from Equation 4 after accounting for the extinction ($A_V$ = 0.44) determined from the color excess given in section 3.1. This corresponds to a distance of 613 pc.

This study has shown that ASAS J184708-3340.8 is well described as a W Ursae Majoris overcontact binary with a filling factor $\mathcal{F}$ = 0.151, and both eclipses passing through totality with an inclination of $i$ = 88.1º ± 0.2. Surface temperatures for the stellar components do differ, and possibly indicate that the system is in poor thermal contact. Additional spectroscopic follow-up will be necessary to place further constraints on the spectral types, stellar masses, and orbital velocities to better improve our knowledge of the system.

## References


Alencar, S. H. P., and Vaz, L. P. R. 1997, *Astron. Astrophys.*, **326**, 257.

Alencar, S. H. P., Vaz, L. P. R., and Nordlund, Å. 1999, *Astron. Astrophys.*, **346**, 556.

Berry, R., and Burnell, J. 2005, *Handbook of Astronomical Image Processing*, Willmann-Bell, Richmond.

CBA Belgium Observatory. 2011, PERANSO (v2.51) software, Flanders, Belgium (http://www.cbabelgium.com/).

Diaz-Cordoves, J., and Gimenez, A. 1992, *Astron. Astrophys.*, **259**, 227.

Fitzgerald, M. P. 1970, *Astron. Astrophys.*, **4**, 234.

Flower, P. J. 1996, *Astrophys. J.*, **469**, 355.

Høg, E., *et al.* 2000, *Astron. Astrophys.*, **355**, L27.

Klinglesmith, D. A., and Sobieski, S. 1970, *Astron. J.*, **75**, 175.

Kwee, K. K., and van Woerden, H. 1956, *Bull. Astron. Inst. Netherlands*, **12**, 327.

Lucy, L. B. 1967, *Z. Astrophys.*, **65**, 89.

Pojmański, G. 1997, *Acta Astron.*, **47**, 467.

Pojmański, G. 2002, *Acta Astron.*, **52**, 397.

Pojmański, G. 2003, *Acta Astron.*, **53**, 341.

Pojmański, G., and Maciejewski, G. 2004, *Acta Astron.*, **54**, 153.

Pojmański, G., and Maciejewski, G. 2005, *Acta Astron.*, **55**, 97.

Pojmański, G., Pilecki, B., and Szczygiel, D. 2005, *Acta Astron.*, **55**, 275.

Prša, A., and Zwitter, T. 2005, *Astrophys. J.*, **628**, 426 (PHOEBE software package v0.31a).

Rucinski, S. M. 1969, *Acta Astron.*, **19**, 245.

Rucinski, S. M., and Duerbeck, H. W. 1997, *Publ. Astron. Soc. Pacific*, **109**, 1340.

Schlafly, E. F., and Finkbeiner, D. P. 2011, *Astrophys. J.*, **737**, 103.

Schwarzenberg-Czerny, A. 1996, *Astrophys. J., Lett. Ed.*, **460**, L107.

van Hamme, W. 1993, *Astron. J.*, **106**, 2096.

Wilson, R. E., and Devinney, E. J. 1971, *Astrophys. J.*, **166**, 605.